PHYSICAL REVIEW B VOLUME 15, NUMBER 1 1 JANUARY 1977

ESR and uniaxial stress study of a freely librating elastic dipole*

Dirk Schoemaker and Ad Lagendijk
Physics Department, University of Antwerp (UIA), 2610-Wilrijk, Belgium †
and Argonne National Laboratory, Argonne, Illinois 60439
(Received 28 June 1976)

Uniaxial stress along ⟨110⟩ lifts the degeneracy of the three tunneling orientations of the restricted interstitial motion of the $H_A(Li^+)$ center in KCl:Li^+. This phonon-assisted tunneling motion possesses C_{3v} symmetry around ⟨111⟩. These experiments yield two differential stress coupling coefficients, which is not sufficient for a determination of the elastic dipole tensor. Uniaxial stress along ⟨100⟩ changes the $H_A(Li^+)$ orientation in a continuous fashion along a well-defined path. An interpretation of the ⟨110⟩ and ⟨100⟩ data is presented. To this end the concept of a free elastic dipole in a stress field is introduced and the statistics of these dipoles are calculated. This permits an interpretation and analysis of the ⟨100⟩ stress data and a third independent linear stress coupling coefficient is obtained. The resulting elastic dipole tensor has a principal axis close to ⟨111⟩. The free elastic dipole model implies that at zero applied stress the Cl_2^- of $H_A(Li^+)$ librates freely over a large angle, i.e., that all positions along the path are equally probable. A careful reanalysis of the ESR spectra has confirmed the existence of this librational motion. The Cl_2^- librates freely with respect to a {110} plane along an almost quadrant of a cone around ⟨100⟩ whose apex angle is $2 \times 28.2°$. The libration frequency is fast enough to result in a motionally averaged but still anisotropic ESR spectrum.

I. INTRODUCTION

The $H_A(Li^+)$ center[1] in KCl:Li^+ possesses two[2] reorientation motions. One of these, the restricted interstitial motion (RIM) of C_{3v} symmetry around ⟨111⟩, exhibits tunneling properties at liquid-helium temperatures and these have been studied by investigating the effect of uniaxial stress $\vec{\sigma}$ on the electron-spin-resonance (ESR) spectra.

In a recent paper[3] the $\vec{\sigma} \| \langle 100 \rangle$ data were presented and an unexpected result was found: ⟨100⟩ stress at 4.2 K changes the orientation of the $H_A(Li^+)$ center in a continuous fashion along a well-defined path, and this overwhelms the effect that the ⟨100⟩ stress should have on the degeneracy of the RIM tunneling orientations. Furthermore, raising the temperature above 4.2 K while high ⟨100⟩ stress is applied, undoes the effect of the ⟨100⟩ stress.

In the first half of this paper (Sec. II) the $\vec{\sigma} \| \langle 110 \rangle$ data will be presented.[4] It will be shown that ⟨110⟩ stress does lift the degeneracy of the three RIM tunneling orientations. In the second half (Sec. III) an interpretation of the ⟨100⟩ and ⟨110⟩ data is presented. This is based on a model of a freely librating elastic dipole in a stress field, and permits the determination of the $H_A(Li^+)$ elastic dipole tensor (Sec IV). The implications of this model and its justification are presented at the end of this paper.

It should be pointed out that as a result of the analysis presented in this paper an important correction has to be applied to the $H_A(Li^+)$-center model.[1,2] However, the analysis given in Secs. II and III A is based on the "old" $H_A(Li^+)$-center model. This has no consequences for the discussion or the results because it will become clear that the "old" model is in some sense an average of the newly proposed model. Thus the presentation in this paper will be along the chronological development of the subject. The refined new model for the $H_A(Li^+)$ center will emerge in Secs. III and IV. The experimental details are the same as in previous papers.[1,2]

II. ⟨110⟩ UNIAXIAL STRESS EXPERIMENTS

A. Tunneling orientations

Because of their complexity it will be useful to recall the model of the $H_A(Li^+)$ center[1] and the geometry of the restricted interstitial motion[2] (RIM). The $H_A(Li^+)$-center model is presented in Fig. 1: A Cl_2^- molecule ion composed from the chlorines Nos. 1 and 2 occupies a single negative ion site next to a substitutional impurity Li^+ ion in the KCl lattice. The Cl_2^- makes a $\theta'' = 26°$ angle with ⟨100⟩ in a {110} plane through this direction. (Later in the paper this angle will be modified to $\theta'' = 28.2°$.) The Li^+ ion lies in this {110} plane, and although it is drawn on a lattice site in Fig. 1, its exact position with respect to the nuclei of the Cl_2^- is not known and cannot be derived from the ESR data as such.

The center also possesses very weak molecular bonds with substitutional Cl^- ions Nos. 3 and 4 in Fig. 1. These are responsible for the nonresolved superhyperfine structure (shf) of the ESR lines. The direction of these weak bonds is indicated by the broken lines in the figure.

These two chlorines, Nos. 3 and 4, together with

Cl No. 2 in Fig. 1 play an important role in the RIM which is shown in Fig. 2. Interstitial Cl No. 1 breaks its molecular bond with Cl^- ion No. 2 and reestablishes a Cl_2^- molecular bond with No. 3 (or No. 4) and so on. This motion possesses C_{3v} symmetry around ⟨111⟩ and is a phonon-assisted tunneling motion at very low temperatures.[2] For clarity the shf directions have not been drawn in Fig. 2.

Uniaxial stress along ⟨110⟩ will be applied so that the degeneracy of the three RIM tunneling orientations will be lifted. In order to understand the stress measurements to be presented in Sec. II B, all the RIM tunneling systems which are inequivalent with respect to a given ⟨110⟩ stress direction must be distinguished. Inspection of all possibilities leads, e.g., $\vec{\sigma} \| [1\bar{1}0]$, to the two inequivalent tunneling systems A and B shown in Fig. 2. In tunneling system A, the RIM takes place around $[1\bar{1}1]$ which makes a 35.26° angle with $[1\bar{1}0]$, whereas for B the motion takes place around [111] which makes a 90° angle with $[1\bar{1}0]$.

Tunneling systems A and B are each representative of a set of two equivalent tunneling systems. The A' system is derived from A by a reflection in the $(1\bar{1}0)$ plane; B' is obtained from B by reflection in the (110) plane. These equivalent sets are not drawn in Fig. 2, but they should be kept in mind.

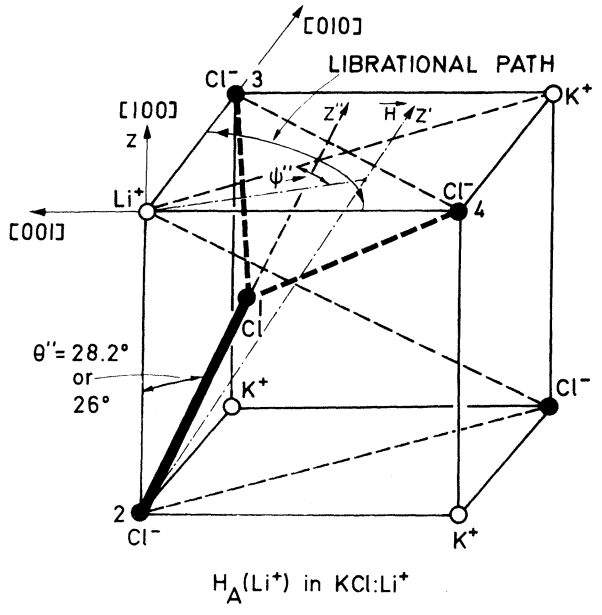

FIG. 1. Schematic three-dimensional model of the $H_A(Li^+)$ center in KCl:Li^+. The midpoint of the 1-2 internuclear axis of Cl_2^- should be near lattice site 2, but this schematic presentation is useful in the discussions. This figure is consistent with Fig. 2(a) and Fig. 8.

Note that the A and B sets are related to each other by a 90° rotation around [001].

Our experimental setup was limited to the $\vec{\sigma} \perp \vec{H}$ configuration. Consequently, in the $\vec{\sigma} \| [1\bar{1}0]$ uniaxial-stress experiments the external magnetic field $\vec{H}$ could only turn in the $(1\bar{1}0)$ plane perpendicular to the stress direction. The angle θ' between $\vec{H}$ and [001] (see Fig. 2) will be used to describe the orientation of the crystal and to characterize the ESR spectra. It is important to visualize and discern all the $H_A(Li^+)$ orientations for different values of θ', and this information is presented in Table I. A Cl_2^- direction defined by nuclei 1 and 2 in system A is indicated by $12A$, etc.

B. Qualitative effect of ⟨110⟩ stress

In order to study the effect of ⟨110⟩ uniaxial stress, one would like to observe isolated well-defined ESR lines corresponding to the various orientations $12A$, $12A'$, ..., $14B$, $14B'$. Unfortunately, this is not possible for two reasons. First, the experimental set up was limited to the $\vec{\sigma} \perp \vec{H}$ configuration.[3,4] This means, e.g., that one cannot observe isolated ESR lines corresponding to the $12B$, $13B$, $12B'$, $13B'$ orientations. Indeed by varying θ' from 0° to 90° the angle θ between $\vec{H}$ and these four directions is never smaller than 63.1°. Such large angles give rise to contracted ESR spectra whose lines are distorted by, or buried under, the lines of spectra with smaller θ.

Second, the ESR lines are broad (at least[1] 7.5 G) and this together with the presence of Cl_2^- of other isotopic combinations ($^{35}Cl\,^{37}Cl^-$) makes that one has to turn over a rather large θ' angle in order

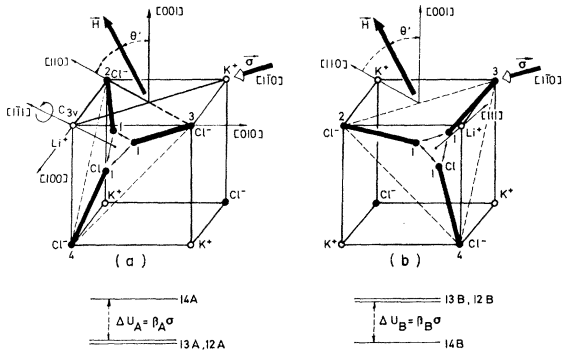

FIG. 2. (a) Schematic presentation of the restricted interstitial tunneling motion (RIM) of C_{3v} symmetry around $[1\bar{1}1]$ for the $H_A(Li^+)$ center in KCl : Li^+. (b) A second RIM system around [111] which is different from (a) with respect to the applied $\vec{\sigma} \| [1\bar{1}0]$ uniaxial stress. Below each system the lifting under $[1\bar{1}0]$ stress of the degeneracy of the three tunneling orientations is given.

to separate clearly lines which are degenerate when $\vec{H}$ is parallel to one of the directions ⟨100⟩, ⟨110⟩, or ⟨111⟩.

The best one can achieve is shown by the ESR spectrum in Fig. 3(a). This presents part of the high-field pattern of the ESR lines corresponding to the crystal orientation $\theta' = 24°$ (Table I).

For this orientation the ESR lines corresponding to directions $14A$, $14A'$, and $14B$ (namely, the $\theta = 34.8°$ and $\theta = 2°$ spectra) are best resolved from one another and from $\theta = 50°$ and $\theta = 50.9°$ originating from directions $14B'$, $12A$, and $12A'$. Unfortunately, isolated lines corresponding to directions $12B'$, $13B'$, $12A$, $14A'$, and $14B'$ cannot be observed simultaneously with $13A$ and $14B$. One can observe $12A$ and $13A$ if $\vec{H}$ is turned to the [110] direction (i.e., when $\theta' = 90°$). However, the study of the effect of ⟨110⟩ uniaxial stress on these orientations is complicated by the fact that this type of uniaxial stress changes the line shapes of the $\theta = 31.3°$ ESR lines[5] and as a result their height cannot be taken as a measure for their intensity.

Figure 3(b) presents the effect of applied $[1\bar{1}0]$ uniaxial stress at 4.2 K and for the $\theta' = 24°$ direction. It is very clear that line $14B$ has increased

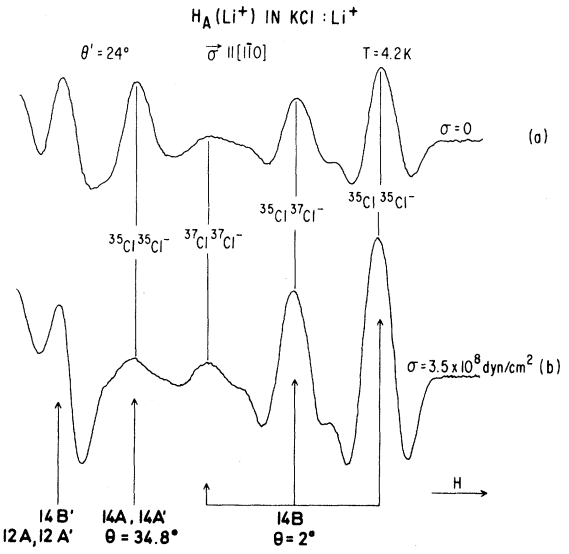

FIG. 3. Part of the high-field side of the $H_A(Li^+)$ ESR spectrum for $\theta' = 24°$ (see Fig. 2 and Table I) showing the effect of $\vec{\sigma} \parallel [1\bar{1}0]$ uniaxial stress on the RIM. (a) No stress at 4.2 K; (b) with ⟨110⟩ stress at 4.2 K.

TABLE I. Orientations θ of the internuclear Cl_2^- axes of the $H_A(Li^+)$ centers for a few orientations of the crystal defined by the angle θ' in Fig. 2. The A' orientations are derived from the A orientations by reflection in the $(1\bar{1}0)$ plane, and B' from B by reflection through (110). A 1-2 direction of system A is written $12A$, etc. This table is based on the "old" $H_A(Li^+)$ center model (see text).

Orientation of crystal with respect to $\vec{H}$	Direction of $H_A(Li^+)$	Angle θ of Cl_2^- axis with magnetic field $\vec{H}$
$\theta' = 0$	$14A, 14A'$	26°
($\vec{H} \parallel [001]$)	$14B, 14B'$	
	$12A, 12B'$	71.9°
	$13A, 13A'$	
	$12B, 12B'$	
	$13B, 13B'$	
$\theta' = 90°$	$12A, 12A'$	31.3°
($\vec{H} \parallel [110]$)	$13A, 13A'$	
	$12B, 12B'$	65.4°
	$13B, 13B'$	
	$14B, 14B'$	64°
	$14A, 14A'$	90°
$\theta' = 24°$	$12A, 12A'$	50.9°
	$12B, 13B$	63.1°
	$12B', 13B'$	83.5°
	$14A, 14A'$	34.8°
	$13A, 13A'$	86.3°
	$14B$	2°
	$14B'$	50°

in intensity while the twofold degenerate $14A$, $14A'$ line has dropped. This substantiates the earlier conclusion[2] that the RIM is still going on at 4.2 K. This spectrum shows that the degeneracy of the RIM tunneling orientations of the two inequivalent tunneling systems A and B is lifted as shown in Figs. 2(a) and 2(b).

C. Quantitative analysis

1. $\theta' = 24°$ experiments

The populations of the tunneling states whose degeneracy is lifted by the ⟨110⟩ uniaxial stress are governed by the Boltzmann distribution. The intensities of the ESR lines are a direct measure for these populations. For system A the intensities of ESR lines $14A$ and $13A$ (the latter degenerate with $12A$) are related by

$$I(14A)/I(13A) = \tfrac{1}{2} e^{-\Delta U_A / k_B T}, \quad (1)$$

in which $\Delta U_A = U(14A) - U(13A)$ is the energy difference caused by the application of the $[1\bar{1}0]$ uniaxial stress and k_B is the Boltzmann constant. Similarly for the system B

$$I(14B)/I(13B) = \tfrac{1}{2} e^{+\Delta U_B / k_B T}, \quad (2)$$

in which $\Delta U_B = U(13B) - U(14B)$ and we have also taken into account the fact that excited state $13B$ remains degenerate with $12B$ under $[1\bar{1}0]$ stress.

In analyzing the experimental data the usual assumption is made that the dependence of the ener-

gies U on the magnitude σ of the applied uniaxial stress is linear:

$$U = \beta\sigma .$$

This relation defines the "linear stress coupling coefficient" β which has the dimension of a volume. Consequently, the energy differences ΔU are also linear functions of σ, and

$$\Delta U_A = \beta_A\sigma \equiv \beta_{[110]}\sigma , \quad \Delta U_B = \beta_B\sigma \equiv \beta_{[1\bar{1}0]}\sigma , \tag{3}$$

define the "differential stress coupling coefficients" β_A and β_B. The equivalent $\beta_{[110]}$ and $\beta_{[1\bar{1}0]}$ notation, which we will use later on, expresses the fact that the A and B sets are related to each other by a 90° rotation around [001].

The only directions that can be studied reliably are $14A$, $14A'$, and $14B$ [Figs. 3(a) and 3(b)]. It was carefully verified experimentally that their line shape was not noticeably influenced by the stress. However, the uniaxial stress does affect the spin-lattice relaxation time T_1 and/or the spin-diffusion time. At the higher microwave powers and at 4.2 K, the $\vec{\sigma} \| \langle 110 \rangle$ stress has the result of increasing the ESR line intensity more than can be accounted for by the effect of the stress on the populations of the tunneling orientations. To eliminate this unwanted contribution the stress experiments were performed at the lowest possible microwave powers and at the lowest possible 100-kHz field-modulation amplitudes for which still an acceptable signal-to-noise ratio was obtained. About 0.1 mW of microwave power and modulation amplitudes in the neighborhood of 1 G peak to peak were used. At these low microwave powers the unwanted effects were strongly reduced, but probably not completely eliminated. We return to this in Sec. III.

For the determination of β_A and β_B we cannot use Eqs. (1) and (2) as such. They can be rewritten, however, as a function of $I(14A)$ and $I_0(14A)$ or $I(14B)$ and $I_0(14B)$, where I_0 represents the starting intensity of a line. One finds, arranging it so that the lines go through the origin, that for line $14A$

$$\ln \frac{2I(14A)}{3I_0(14A) - I(14A)} = -\frac{\beta_A\sigma}{k_B T} , \tag{4}$$

and similarly for line $14B$

$$\ln \frac{3I_0(14B) - I(14B)}{2I(14B)} = -\frac{\beta_B\sigma}{k_B T} . \tag{5}$$

The experimental plots for $T = 4.2$ K and ~0.1 mW are given in Fig. 4. The assumed linear relationship between ΔU and σ is indeed verified and from the slopes one deduces the following values for the differential stress coupling coefficients:

$$\beta_A = (2.9 \pm 0.2) \times 10^{-24} \text{ cm}^3 , \tag{6}$$
$$\beta_B = (2.1 \pm 0.2) \times 10^{-24} \text{ cm}^3 .$$

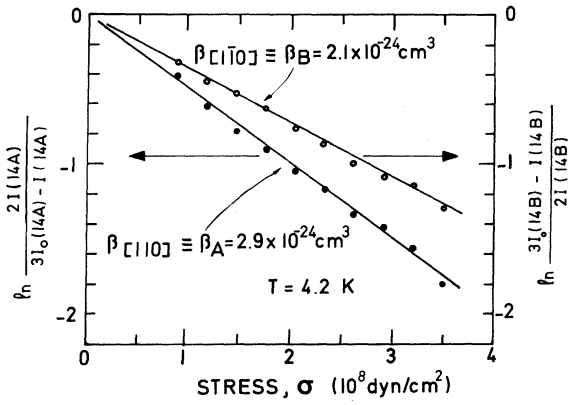

FIG. 4. Population-vs-σ plot yielding the two differential stress coupling coefficients for $\vec{\sigma} \| \langle 110 \rangle$.

Similar experiments at a few temperatures up to about 12 K show that the slopes of the lines are proportional to $1/T$. This is as it should be if the Boltzmann distribution holds.

The results of Fig. 4 are representative of several independent measurements on different samples. In all experiments of this type (i.e., $\theta' = 24°$) it was found that $\beta_A > \beta_B$ and the foregoing values were quite reproducible within the stated limits. Even so, one must be cautious. First, one would feel more confident if the β's had been obtained from formulas (1) and (2) rather than formulas (4) and (5). Second, the experimental results indicate that even at ~0.1 mW there still seems to be an effect of σ on T_1 (see following), and one cannot discard the possibility that the effect of σ on T_1, exhibits an anisotropy. These, and possible other unrecognized experimental effects may produce errors in the magnitudes and relative magnitude of β_A and β_B. That these apprehensions may be founded is shown by the $\vec{H} \| [001]$ experiments ($\theta' = 0°$) to be discussed below.

2. $\theta' = 0°$ experiments ($\vec{H} \| [001]$)

For the $\theta' = 0°$ orientation of the crystal, i.e., when $\vec{H} \| [001]$, the $14A$ and $14B$ spectra coincide to give a fourfold-degenerate $\theta = 26°$ spectrum. The effect of the $\vec{\sigma} \| [1\bar{1}0]$ stress on this spectrum will be a balance between the two degenerate $14A$ lines going up and the two degenerate $14B$ lines going down. Using the values for β_A and β_B as given by (6) one calculates that the $\theta = 26°$ line intensity should *decrease* by about 5% at 4.2 K when the magnitude of the $\vec{\sigma} \| [1\bar{1}0]$ stress is about 2.9×10^8 dyn/cm^2.

However, the experiment gives a 5% *increase* in line intensity for this stress and at ~0.1 mW. (At ~25 mW and 4.2 K one finds an increase of about 50% clearly indicating an effect of σ on T_1.) This

was carefully checked by a double integration of the first-derivate line. In this experiment it was also verified that the 26° line shape was quite accurately Gaussian and unaltered by the ⟨110⟩ stress. These results imply that $\beta_A > \beta_B$, which is in contradiction with the results of Sec. II C1. We conclude that some of the perturbing effects suggested at the end of Sec. II C1 may indeed be present possibly together with other unrecognized effects. The best one can say is that $\beta_A \approx \beta_B$ or

$$\beta_{[110]} = \beta_{[1\bar{1}0]} = (2.5 \pm 0.4) \times 10^{-24} \text{ cm}^3, \tag{7}$$

which is the average of the differential stress coupling values given in expression (6).

Finally, it should be mentioned that a small number of exploratory uniaxial stress measurements were performed with $\vec{\sigma} \| \langle 111 \rangle$. One might expect a mixture of $\vec{\sigma} \| \langle 100 \rangle$ and $\vec{\sigma} \| \langle 110 \rangle$ effects, i.e., an effect on both the lifting of the degeneracy of the RIM tunneling orientations[2] and on the geometric structure.[3] The exploratory investigation did bear this out. However, because of the complexity of the ESR spectra and because of the limitations in the experimental stress geometry ($\vec{\sigma} \| \langle 111 \rangle \perp \vec{H}$) a detailed analysis was not attempted.

III. ELASTIC DIPOLE TENSOR OF H_A (Li^+)

A. Analysis of $\vec{\sigma} \| \langle 110 \rangle$ data

The influence of an external applied stress (tensor) field on the physical properties of a solid can be described by various models, the simplest being the classical continuum theory of an elastic solid.[6-9] This continuum model is particularly useful to account for the lifting of the orientational degeneracy of a low-symmetry defect in a high-symmetry solid by an applied uniaxial stress. An interesting situation arises when a low-symmetry defect exhibits motions at low temperatures which enables it to jump to any, or part, of its equivalent positions. In that case a removal of the orientational degeneracy by a stress field will lead to different populations for the various orientations of the defect as determined by Boltzmann's distribution law.

Within the continuum approach one can formulate the concept of the "elastic dipole tensor"[7,8] of a defect, which represents the lattice distortion around the defect in terms of the change of the macroscopic strain due to the introduction of the defects. Another equivalent formulation appeals to the "double force tensor,"[8] which defines a force distribution which would distort the *perfect* lattice in the same way as the defect does.

The elastic free enthalpy density of a perfect solid can be expressed[9]

$$U = -\tfrac{1}{2}\vec{\sigma} \cdot \vec{e} = -\frac{1}{2}\sum_{i,j} \sigma_{ij} e_{ij}, \tag{8}$$

where $\vec{\sigma}$ denotes the stress tensor, $\vec{e}$ is the strain tensor, and i, j run over the Cartesian components x, y, and z. The influence of the defects can be accounted for by modifying the strain. For a sufficiently low concentration the strain can be expanded in powers of the defect concentration as

$$e_{ij}(n) = e_{ij}(0) + n\left(\frac{\partial e_{ij}}{\partial n}\right)_{n=0} + \cdots, \tag{9}$$

with n the number of defects per unit volume. The dimensionless "$\vec{\lambda}$ tensor" or "elastic dipole tensor" is defined by

$$\lambda_{ij} = \frac{1}{V_0}\left(\frac{\partial e_{ij}}{\partial n}\right)_{n=0}, \tag{10}$$

in which V_0 represents the molecular volume of the matrix crystal. Combination of Eqs. (8)–(10) tells us that the interaction of the elastic dipole with the stress field is represented by

$$\Delta U = -V_0 \vec{\lambda} \cdot \vec{\sigma} \equiv \vec{\beta} \cdot \vec{\sigma}, \tag{11}$$

in which $\vec{\beta}$ represents the linear stress coupling tensor. The interaction energy of Eq. (11) is per unit volume, and per unit defect concentration, i.e., per defect. The information which should be extracted from experiment are the three principal values and the three principal directions of the second-rank $\vec{\lambda}$ tensor. The double-force-tensor method[8] characterizes the effect of the introduction of imperfections by a force distribution. To this end the stress tensor $\vec{\sigma}$ in Eq. (11) is replaced by the stress-induced strain tensor $\vec{e}$ employing Hooke's law. The result is

$$\Delta U = -V_0 \vec{C} \cdot \vec{\lambda} \cdot \vec{e} \equiv -\vec{P} \cdot \vec{e}, \tag{12}$$

where $\vec{P}$ is the double force tensor, and $\vec{C}$ is the fourth-order tensor of the elastic moduli of the solid. $\vec{P}$ is the force array which would produce in the *perfect* lattice the same macroscopic lattice distortion as the defect does. The elastic moduli near the defect can be, and probably are, quite different from those of the perfect solid explaining the restriction made in the interpretation of $\vec{P}$.

Because they were introduced using the continuum approximation both the $\vec{\lambda}$ and $\vec{P}$ tensors are macroscopic quantities, i.e., they are defined over volumes much larger than the molecular-defect volume. They are able to describe the interaction of a macroscopic defect-induced strain field $\vec{\lambda}$, or a macroscopic defect-induced stress field $\vec{P}$, with the external stress-induced strain. The extraction of these quantities from an atomistic calculation is very difficult. In order to do so one has to calculate the displacements over

large distances around the defect and fit these to a displacement ellipsoid. Conversely, the extrapolation of these tensors to a microscopic, i.e., atomistic, scale should be performed with caution.

However, the $\vec{\lambda}$ tensor is the quantity which is directly observed experimentally and this makes it a meaningful quantity to attempt to extrapolate to atomic dimensions. The $\vec{P}$ tensor on the other hand is derived from $\vec{\lambda}$ using the macroscopic compliance coefficients and this accentuates the macroscopic character of the $\vec{P}$ tensor. One should, therefore, not be too eager to attempt to give the double force tensor a microscopic interpretation. For this reason we prefer to use the $\vec{\lambda}$ tensor and will not use the $\vec{P}$ tensor.

The elastic dipole tensor can be divided into an isotropic part and a traceless anisotropic part. Experiments such as optical polarization which detect the *difference* in population of the elastic levels involve only the anisotropic part $\vec{\lambda}'$ of the elastic dipole tensor. Consequently, we are only able to determine, not $\vec{\lambda}$, but its anisotropic part, $\vec{\lambda}'$, whose principal values are subject to the condition $\lambda_1' + \lambda_2' + \lambda_3' = 0$. The isotropic part of $\vec{\lambda}$ merely corresponds to the fractional volume increase or decrease caused by the defect.

The majority of experiments performed to measure the elastic dipole tensor of defects involve rather high-symmetry defects, e.g., a tetragonal defect in a cubic solid. This simplifying situation is an almost necessary restriction for the experiments to be analyzable. Let us take a cubic solid, and introduce an arbitrarily oriented defect, and let us apply a uniaxial stress along an arbitrary direction. There will be twelve nonequidistant elastic energy levels. The thermal behavior of such a manifold is so complicated that it will be difficult to distill the elastic dipole tensor from it. There are, however, two types of possible simplifications: (i) the symmetry of the defect is so high that all the directions of the $\vec{\lambda}$ tensor are dictated by the symmetry alone and uniaxial stress along high-symmetry axes results in two-level systems which can be analyzed easily,[8] yielding the principal values, or, (ii) the thermal transitions between certain orientations are not allowed, which may result in a simpler thermal behavior. The $H_A(\mathrm{Li}^+)$ center in KCl:Li^+ is an example of the second simplification: There is no communication between the orientations of the two tunneling systems A and B, because the "pryamidal motion"[2] (PM) does not exist at low temperatures (<23.5 K). It is exactly this lack of communication which gives the simple two-level systems for $\vec{\sigma} \| \langle 110 \rangle$ stress whose thermal behavior was analyzed in detail in the first part of this paper. The $H_A(\mathrm{Li}^+)$ center in NaF:Li^+, which possesses no symmetry elements,[10] is an illustration of a system in which all thermal transitions appear allowed, resulting in a very complicated response to external stress.[11] In the majority of cases there are no thermal transitions between equivalent orientations at all at low temperatures owing to the heights of the barriers.

We will now attempt to determine the principal axes and principal values of the elastic dipole tensor of $H_A(\mathrm{Li}^+)$ and we will use the $H_A(\mathrm{Li}^+)$ model as depicted by the Cl_2^- in the 1-2 orientation in Fig. 2(a). We start by noting that the symmetry of $H_A(\mathrm{Li}^+)$ is C_{1h} forcing one of the principal axes, ξ say, to be along the normal [011] of the (011) reflection plane. The other two principal directions will be called η and ζ and both lie in the (011) plane. Their orientations are defined by the angle α which η makes with the $[0\bar{1}1]$ direction.

For uniaxial stress applied along $[1\bar{1}0]$ we obtained in (7) two differential stress coupling coefficients $\beta_{[110]}$ and $\beta_{[1\bar{1}0]}$ and a straightforward calculation yields

$$\begin{aligned}\beta_{[110]} &= V_0[\lambda'_{\xi\xi}(1 + \tfrac{1}{4}\cos^2\alpha + \sin 2\alpha/2\sqrt{2}) \\ &\quad + \lambda'_{\eta\eta}(\tfrac{1}{4}\cos 2\alpha + \sin 2\alpha/\sqrt{2})], \\ \beta_{[1\bar{1}0]} &= V_0[\lambda'_{\xi\xi}(1 - \tfrac{5}{4}\cos^2\alpha + \sin 2\alpha/2\sqrt{2}) \\ &\quad + \lambda'_{\eta\eta}(-\tfrac{5}{4}\cos 2\alpha + \sin 2\alpha/\sqrt{2})],\end{aligned} \tag{13}$$

in which $\lambda'_{\xi\xi}$, $\lambda'_{\eta\eta}$, together with $\lambda'_{\zeta\zeta}$ are the principal values of the traceless tensor $\vec{\lambda}'$. It is clear we cannot determine $\vec{\lambda}'$ and its orientation from Eqs. (13). We need another independent stress coupling coefficient. This we shall obtain in Sec. III B but we can give already a good qualitative argument which shows that α is expected to be in the neighborhood of 35.26°, i.e., that α should be near $\langle 111 \rangle$. (In Sec. III B it will be shown that $\alpha = 39°$.)

Indeed, for interstitial centers one expects rather large λ' and λ principal values because one extra atom is squeezed into the crystal and because the symmetries of the centers are lower than cubic. This expectation is supported by the comparison of the $\vec{\lambda}'$ tensors of the V_K and H centers[8,12] both of which possess D_{2h} symmetry in KCl. They are presented in Table II. The principal values of $\vec{\lambda}'$ for the interstitial H center are a few times larger than those of the substitutional V_K center although in both cases the same molecular ion Cl_2^- in the same crystal KCl is involved.

For the interstitial $H_A(\mathrm{Li}^+)$ center large values are thus expected for the stress coupling coefficients. However, because Li^+ is smaller than K^+, these coefficients should be smaller than those of

TABLE II. Anisotropic part $\tilde{\lambda}'$ of the elastic dipole tensor of the H center, the V_K center, and the $H_A(Li^+)$ center in KCl.

	λ_1'	λ_2'	λ_3'	
H center[a]	0.47	−0.62	0.15	Ref. 8
V_K center[a]	0.11	−0.11	0	Ref. 12
$H_A(Li^+)$[b]	−0.11	0.33	−0.22	This work

[a] The directions 1, 2, and 3 denote ⟨110⟩ perpendicular to molecular axis, ⟨100⟩ perpendicular to molecular axis, and the molecular axis, respectively.

[b] The directions 1, 2, and 3 denote ξ, η, and ζ as defined in the text; the angle α between η and $[1\bar{1}0]$ is found to be 39° (see also Fig. 8).

the H center.

We can vary α from 0° to 90° in Eqs. (13) and solve for $\lambda'_{\xi\xi}, \lambda'_{\eta\eta}, \lambda'_{\zeta\zeta}$, and see where these values become large so that they could give larger β's than the two already determined. It turns out that these three principal λ' values are quite small and slowly varying everywhere, except when α is in the neighborhood of 35.26°. The results around this angle are plotted in Fig. 5. (The infinities in this figure have no physical meaning. In order to obtain finite λ' values at $\alpha = 35.26°$ the experimental ratio $\beta_{[1\bar{1}0]}/\beta_{[110]}$ should be three.) This plot clearly shows that for large λ' values, i.e., large β values, α should be close to 35.26°. That the ⟨111⟩ should be an important orientation for $H_A(Li^+)$

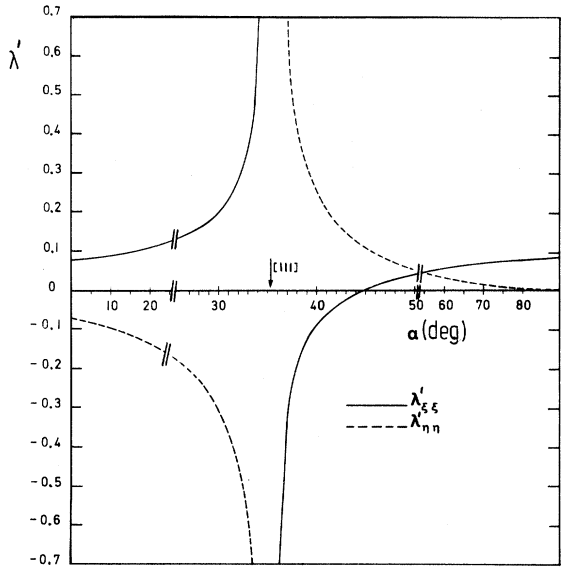

FIG. 5. Components $\lambda'_{\xi\xi}$ and $\lambda'_{\eta\eta}$ of the anisotropic part of the elastic dipole tensor vs the angle α between $[0\bar{1}1]$ and the η axis of the dipole, as derived from Eqs. (13) and the differential stress coupling coefficients as given by (7).

is not surprising: the RIM takes place around ⟨111⟩. Furthermore, from an inspection of the $H_A(Li^+)$ model in Fig. 1 it can be remarked that the important part of the defect determining the elastic properties of $H_A(Li^+)$ is very likely composed out of the Li^+ ion and the interstitial chlorine No. 1. From the very schematic presentation in Fig. 1 one might infer that the axis Li^+–Cl No. 1 is likely to be close to a ⟨111⟩ direction, and, if an extrapolation to macroscopic dimensions is allowed, that one of the $\tilde{\lambda}'$-tensor axes should be in the neighborhood of ⟨111⟩.

B. Interpretation of continuous change in orientation under ⟨100⟩ stress

The argument given in Sec. III A, establishing the approximate orientation of the elastic dipole, is, we believe, a reasonable one. Another independent stress coupling coefficient, linear or differential, from $\tilde{\sigma} \| [001]$ experiments, could confirm this and would provide a better fix on the orientation of the elastic dipole.

However, as was shown in a previous paper,[3] the response of the $H_A(Li^+)$ center to $\tilde{\sigma} \| \langle 100 \rangle$ stress is rather unusual and can be summarized as follows. At 4.2 K the application of [001] stress results in a movement of, e.g., the 1-2 Cl_2^- axis [Fig. 2(a)] out of its (011) plane and with increasing stress it describes an octant of a cone around [100] having a $2 \times 26° = 52°$ apex angle. At high uniaxial stresses ($\sim 5 \times 10^8$ dyn/cm^2) the Cl_2^- axis approaches the (001) plane perpendicular to the stress direction. On the other hand, raising the temperature from 4.2 K with the applied stress on, counteracts the effect of uniaxial stress, i.e., the Cl_2^- returns to its (011) plane.

A formal way to solve this problem is to treat all interactions including the applied stress and to find the potential surface after which the partition function is calculated. This formidable task will not be attempted here. In contrast we will present a simple model which displays the requested temperature and stress dependence and which permits the determination of a third independent linear stress coupling coefficient $\beta^{LM}_{[001]}$. To this end, we make the important observation that the qualitative features of the experimental results[3] are such that they give the impression that the elastic dipole ellipsoid can orient itself in a continuous fashion in a stress field in analogy with, e.g., a classical electric dipole in an electric field.

To illustrate the idea, let us consider a simple case, and let us take, as opposed to an elastic dipole which has because of its symmetry only a discrete number of equivalent positions, an elastic dipole which has a continuous distribution of orien-

tations of equal energy in a plane. The application of stress along a direction in this plane will destroy the equivalence of all these positions and the elastic dipole will orient itself as far as the thermal motions allow it. Employing classical statistical physics enables one to calculate the average orientation of the elastic dipoles characterized by the thermal average of $\cos^2\psi$, ψ being the angle between the stress direction and a principal axis of the elastic dipole in the plane. The anisotropic part of the energy will vary as $\cos^2\psi$, and therefore for this simple model the Hamiltonian is, apart from a constant factor which is irrelevant,

$$\mathcal{H} = -\beta\sigma\cos^2\psi\,, \tag{14}$$

in which σ is the magnitude of the applied external stress and β a linear stress coupling coefficient characterizing the anisotropy of the $\vec{\lambda}$ tensor in the plane in which the reorientation of the elastic dipole takes place. It is a function of the three principal values of the $\vec{\lambda}'$ tensor. The thermal averages of $\cos^n\psi$ are

$$\langle\cos^n\psi\rangle = \left[\int_0^\gamma \exp\left(\frac{\beta\sigma\cos^2\psi}{k_BT}\right)\cos^n\psi\,d\psi\right] \times\left[\int_0^\gamma \exp\left(\frac{\beta\sigma\cos^2\psi}{k_BT}\right)d\psi\right]^{-1}, \tag{15}$$

where γ is the angle over which the ellipsoid can orient itself in the plane.

The phenomena are studied with ESR. Let us assume again for simplicity, that the external magnetic field $\vec{H}$ is parallel to $\vec{\sigma}$ and that the symmetry axis of the spin Hamiltonian coincides with an elastic dipole tensor axis in the plane. As we shall see, the ESR spectra which we measure reflect average values of squared trigonometric functions indicating that we need $\langle\cos^2\psi\rangle$, and, to get an idea of the spread, $\langle\cos^4\psi\rangle$. The experiments on the $H_A(\mathrm{Li}^+)$ center indicate that a $\langle\cos^2\psi\rangle$ varies between $\frac{1}{2}$ and a value close to 1 for zero and infinite temperature, respectively. The orientation or libration range represented by γ can be determined using this observation[13] and this yields approximately $\gamma \leq 90°$. Calculating $\langle\cos^2\psi\rangle$ and $\langle\cos^4\psi\rangle$, e.g., for $\gamma = 90°$, with the help of Eq. (15) is relatively simple and we obtain the following expressions:

$$\langle\cos^2\psi\rangle = \tfrac{1}{2} + \tfrac{1}{2}I_1(\tfrac{1}{2}x)/I_0(\tfrac{1}{2}x) \tag{16}$$

and

$$\langle\cos^4\psi\rangle = \tfrac{3}{8} + [4I_1(\tfrac{1}{2}x) + I_2(\tfrac{1}{2}x)]/8I_0(\tfrac{1}{2}x)\,, \tag{17}$$

in which $x \equiv \beta\sigma/k_BT$ and $I_n(\alpha)$ is the modified Bessel function of order n and argument α.[14] Both averages are depicted in Fig. 6. The qualitative features of the $\langle\cos^2\psi\rangle$ are as expected and exhibit a Langevin-type behavior: Infinite stress ($x = \pm\infty$) causes an alignment of the ellipsoid along the $\psi = 0°$ or the $\psi = 90°$ axis depending on the sign of the linear stress coupling coefficient and on the sign of the stress (compression or tension). Furthermore, infinite temperature ($x = 0$) results in an average value $\langle\cos^2\psi\rangle = \frac{1}{2}$.

We now want to apply the ideas contained in this simple model to the behavior of $H_A(\mathrm{Li}^+)$ under $\langle 100\rangle$ stress. Because the phenomena are studied by ESR we have to look closely into what we are actually measuring.

In the light of the above model the experimental $\vec{\sigma} \| \langle 100\rangle$ data on $H_A(\mathrm{Li}^+)$ are interpreted as a change of the *average* $H_A(\mathrm{Li}^+)$ orientation under uniaxial stress. The experimental evidence indicates[3] that the change of average orientation takes place along an *octant* of a cone around $\langle 100\rangle$ whose apex angle is $2\times 26°$. This means that with stress removed, the Cl_2^- of $H_A(\mathrm{Li}^+)$ moves, or better librates, rather freely along a (almost) *quadrant* of a cone around $\langle 100\rangle$. This motion will be called the libration motion (LM).

One can envisage two extreme experimental situations: (a) the librational frequency is slow compared to the ESR sampling time, or (b) the librational frequency is fast.

In the first case one should see a smeared out, probably unrecognizable, ESR spectrum because the basic $H_A(\mathrm{Li}^+)$ spectrum is strongly anisotropic, and all orientations on the quadrant of the cone are equally probable.

This is definitely not observed. The $H_A(\mathrm{Li}^+)$ spectra are well defined looking like Cl_2^-'s occupying discrete orientations.[1,2] One must conclude therefore that the librational frequency is so fast as to result in motionally averaged ESR spectra.

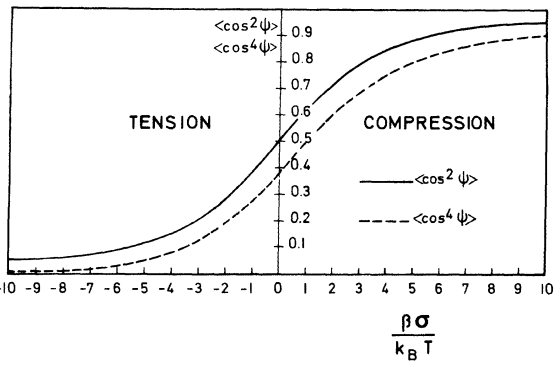

FIG. 6. Theoretical Langevin-type plots based on Eqs. (16) and (17) of an elastic dipole freely librating in a plane and possessing a 90° libration range; $\langle\cos^2\psi\rangle$ describes the average orientation and $\langle\cos^4\psi\rangle$ the spread in average orientation. The figure is based on a positive linear stress coupling constant β.

Since the LM is a limited motion, the resulting averaged ESR spectra must still exhibit a sizeable anisotropy, as is indeed the case.

The formal way to analyze ESR spectra resulting from limited fast motions has been given before.[15] Assuming the following spin Hamiltonian:

$$\frac{\mathcal{H}}{g_0\mu_B} = \frac{1}{g_0}\vec{H}\cdot\vec{g}\cdot\vec{S} + \sum_{i=1}^{2}\vec{S}\cdot\vec{A}_i\cdot\vec{I}_i\,, \tag{18}$$

where the sum is over the two nuclei of the Cl_2^-, the first-order hyperfine (hf) separation and the g anisotropy are given by (assuming axial symmetry)

$$\langle K_i\rangle^2 = [(A_{\parallel,i}-A_{\perp,i})\alpha_i + A_{\perp,i}]^2 + (A_{\parallel,i}-A_{\perp,i})^2(\beta_i^2+\gamma_i^2)\,, \tag{19}$$

$$\langle g\rangle^2 = [(g_\parallel - g_\perp)\alpha_g + g_\perp]^2 + (g_\parallel - g_\perp)^2(\beta_g^2+\gamma_g^2)\,, \tag{20}$$

with,

$$\alpha_i \equiv \langle\cos^2\theta_i\rangle\,,$$
$$\beta_i \equiv \langle\sin\theta_i\cos\theta_i\cos\psi_i\rangle\,, \tag{21}$$
$$\gamma_i \equiv \langle\sin\theta_i\cos\theta_i\sin\psi_i\rangle\,,$$

in which (θ_i, ψ_i) are the polar coordinates of the spin-Hamiltonian symmetry axes with respect to a set of axes (x', y', z') tied to the magnetic field $\vec{H} \parallel z'$. These averages (thermal averages if stress is applied) of the trigonometric functions must be taken over the path of the librational motion.

These expressions should be contrasted with the well-known angular variation formulas which hold when the centers are static (or slowly moving):

$$K^2g^2 = A_\parallel^2 g_\parallel^2\cos^2\theta + A_\perp^2 g_\perp^2\sin^2\theta\,, \tag{22}$$

$$g^2 = g_\parallel^2\cos^2\theta + g_\perp^2\sin^2\theta\,. \tag{23}$$

What these formulas show is that in analyzing motionally averaged spectra one can only determine averages such as, e.g., $\langle\cos^2\theta_i\rangle$, and not θ_i. The latter is only possible for static centers.

The analysis based on the $\vec{\sigma} \parallel \langle 100\rangle$ stress data which resulted in Figs. 7 and 8 in Ref. 3 was based on formulas (22) and (23). In other words, the implicit assumption was made at that time that the observed change in the Cl_2^- orientation under $\langle 100\rangle$ stress was the result of a change in orientation of a static center which remained a static center under stress. With the assumption of large-angle librational motion that we introduce, this is not correct. Formulas (19)–(21) have to be used together with the observed K_i values.

The averages α_i, β_i, and γ_i can be calculated from Eqs. (21) as a function of the linear stress coupling coefficient $\beta^{LM}_{[001]}$ provided one knows the amplitude and path of the librational motion. For instance,

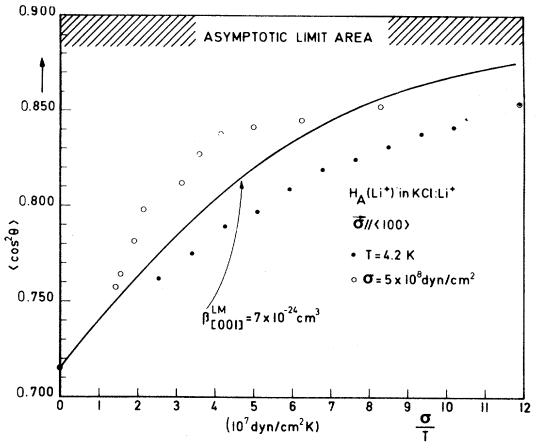

FIG. 7. Experimental Langevin-type plots of the $\vec{\sigma} \parallel \langle 100\rangle$ uniaxial stress data obtained in Ref. 3; the solid line represents an average fit based on $\beta^{LM}_{[001]} = (7\pm2)\times10^{-24}$ cm^3. A fit to the solid points gives $(5\pm0.5)\times10^{-24}$ cm^3 and a fit to the open circles $(9\pm2)\times10^{-24}$ cm^3.

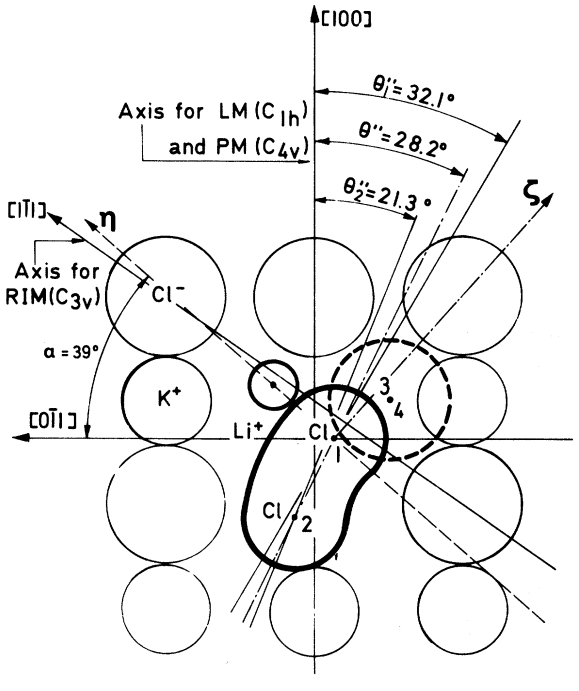

FIG. 8. Two-dimensional model in the (011) plane of the $H_A(Li^+)$ center in KCl:Li^+ incorporating the new results obtained in this paper concerning the g, hyperfine, and elastic dipole tensor axes. The Cl_2^- molecule librates around [100] with respect to the plane of the figure. The libration range is about 70°–80°, and each point along the path is equally probable.

$$\alpha_i \equiv \langle \cos^2\theta_i \rangle = \left(\int_{\psi_a''}^{\psi_b''} e^{-\mathcal{H}/k_B T} \cos^2\theta_i \, d\psi'' \right) \times \left(\int_{\psi_a''}^{\psi_b''} e^{-\mathcal{H}/k_B T} \, d\psi'' \right)^{-1}, \quad (24)$$

in which ψ'' is the angle (Fig. 1) between the planes defined (i) by $\vec{H} \| z'$ and the $\langle 100 \rangle \| z$ direction around which the LM takes place; and (ii) by the $H_A(\mathrm{Li}^+)\ \mathrm{Cl}_2^-$ and the same $\langle 100 \rangle$; ψ_a'' and ψ_b'' define the limits of the LM. When $\vec{H}$ lies in a $\{110\}$ plane, then $\psi_a'' = -\psi_b''$; when $\vec{H}$ lies in a $\{100\}$ plane, $\psi_a'' + \psi_b'' = \frac{1}{2}\pi$. The integration is over ψ'' because all these angles are equally probable when there is no external stress $\vec{\sigma}$. The integration, analytically or numerically, is performed by noting that

$$\cos\theta_i = \cos\theta_i'' \cos\theta' + \sin\theta_i'' \sin\theta' \cos\psi'', \quad (25)$$

in which θ_i'' is the constant angle that the $\vec{K}_i$ tensor makes with $\langle 100 \rangle$ while librating, and θ' the angle that $\vec{H}$ makes with $\langle 100 \rangle$.

The Hamiltonian $\mathcal{H}$ in expression (24) represents the interaction energy of the elastic dipole with the applied $\langle 100 \rangle$ stress field. When $H_A(\mathrm{Li}^+)$ librates along the cone, the axis ξ, which is perpendicular to the Cl_2^--Li^+ plane [the Cl_2^--[100] plane in Fig. 2(a)] remains in the (100) plane which also contains the stress direction. Consequently, the anisotropic part of the interaction energy is

$$\mathcal{H} = -\beta_{[001]}^{\mathrm{LM}} \sigma = -V_0 \sigma \cos^2\varphi \left[\lambda'_{\xi\xi} (\sin^2\alpha + 1) - \lambda'_{\eta\eta} \cos 2\alpha \right], \quad (26)$$

in which $\varphi = \psi'' + \frac{1}{2}\pi$ is the angle between ξ and the $\vec{\sigma} \| [001]$ stress direction, and $\beta_{[001]}^{\mathrm{LM}}$ is the linear stress coupling coefficient.

Our mode of attack in analyzing the data will be the following. The $\vec{\sigma} \| \langle 100 \rangle$ data that yielded Figs. 7 and 8 of Ref. 3 will be reanalyzed using Eqs. (19) and (20) and similar expressions as Eq. (24) for β_i and γ_i. From the experimental $\langle K_i \rangle$ values, values for $\langle \cos^2\theta_i \rangle$ will be derived. For this we need the thermal averages β_i^2 and γ_i^2. But in order to do this we need the spin-Hamiltonian parameters and the θ_i'' values derived from analysis of the ESR data at zero stress, *in which the librational motion is taken into account.* The spin-Hamiltonian parameters obtained before[1,2,4] for $H_A(\mathrm{Li}^+)$ were derived with the assumption that it was a static center, i.e., formulas (22) and (23) were used.

The ESR analysis taking the LM into account is an involved one. It merits separate treatment and is given in the Appendix. It is found that this analysis gives a superior fit to the ESR data when compared with the earlier static analysis. The new ESR results are distinctly different from the static ESR data, and both results are given in the Appendix.

In order to calculate the thermal averages β_i nad γ_i we still need $\beta_{[001]}^{\mathrm{LM}}$. Clearly an iterative procedure must be used. It turns out that $\beta_{[001]}^{\mathrm{LM}} = (7 \pm 2) \times 10^{-24}$ cm^3 and this value was used to calculate the final β_i and γ_i values.

The reasons for calculating β_i and γ_i are (i) that they cannot be determined experimentally from Eqs. (19) and (20) because of insufficient data; and (ii) because they turn out to be small compared to $\langle \cos^2\theta_i \rangle$ (see Appendix).

Using the same stress data that led to Figs. 7 and 8 of Ref. 3, $\langle \cos^2\theta_i \rangle$ was calculated and the results are plotted in Fig. 7. The two sets of data ($T = 4.2$ K and σ varying; $\sigma =$ const and T varying) show the correct qualitative behavior, but they differ from each other. The difference could be real and be caused by, e.g., the stress and temperature dependence of the $\vec{\lambda}$ tensor (which goes beyond the present formulation), but it is also very probable that the difference is caused by experimental errors and by the approximations used in the analysis.[3] We will not discuss it further but try to obtain an average fit for the two sets of data points.

In order to fit one needs the amplitude of the LM. This is given by the limiting value of $\langle \cos^2\theta \rangle$ for $\sigma/T \to \infty$. The data of Fig. 7 are not very precise in this respect but they suggest an asymptotic value for $\langle \cos^2\theta \rangle$ lying around 0.9 or lower. This corresponds to, approximately, $\psi_b'' - \psi_a'' = 80°$ to 70°. With this LM interval one obtains a best fit for the two curves when

$$\beta_{[001]}^{\mathrm{LM}} = (7 \pm 2) \times 10^{-24} \text{ cm}^3. \quad (27)$$

The two curves fit separately give 5×10^{-24} and 9×10^{-24} cm^3, for the lower and upper experimental points, respectively.

With this $\beta_{[001]}^{\mathrm{LM}}$ we can now, using Eq. (26) and Fig. 4, determine the λ' values and the angle α establishing the orientation of the elastic dipole in the $\{110\}$ plane. They are presented in Table II showing in particular that $\alpha = 39°$.

Finally, Fig. 8 presents a schematic two-dimensional model of the $H_A(\mathrm{Li}^+)$ center in the (011) plane. The directions for the hyperfine and elastic dipole tensor and internuclear axes as obtained in this paper have been incorporated. The Cl_2^- librates with respect to this plane around [001].

C. Change of geometry under ⟨110⟩ stress and effect of ⟨100⟩ stress on the RIM tunneling

At first glance the $\langle 100 \rangle$ and $\langle 110 \rangle$ stress data on $H_A(\mathrm{Li}^+)$ are qualitatively quite different: $\langle 110 \rangle$ stress affects the tunneling RIM but does not seem to affect the geometry[16] of the center, whereas $\langle 100 \rangle$

stress affects primarily the geometry to such an extent that it seemingly has no effect on the RIM.

A closer inspection of the $\vec{\sigma} \| \langle 110 \rangle$ data shows however that there is an effect on the geometry. The hf separation at 4.2 K originating from Cl_2^- 1–2 in Fig. 2(a) ($\theta = 31.3°$ spectrum, $\vec{H} \| [110]$, $\vec{\sigma} \| [1\bar{1}0]$ decreases from K = 85.7 G for no stress, to $K = 84.0$ G when $\sigma = 2.9 \times 10^8$ dyn/cm^2. This can be understood by an increase in the average 1–2 Cl_2^- orientation with respect to $\vec{H} \| [110]$. The observed decrease of K corresponds to a change of the average ψ'' value of magnitude $\Delta\psi'' \cong 4°$. This is smaller than expected. Indeed, the $\vec{\sigma} \| [1\bar{1}0]$ stress has a [010] component of magnitude $\frac{1}{2}\sigma$. For $\sigma = 2.9 \times 10^8$ dyn/cm^2 this leads to $\Delta\psi'' \cong 10°$.

The smaller $\Delta\psi''$ values may possibly be explained by noting that the induced strain under $\langle 110 \rangle$ stress is much larger than under comparable $\langle 100 \rangle$ stress because[17] $S_{44} \approx 10 S_{11}$ for KCl. Consequently, it seems likely that $\langle 110 \rangle$ stress will spoil far more quickly than $\langle 100 \rangle$ stress does, the proposed flat potential that the Cl_2^- is moving in. Thus, $\vec{\sigma} \| \langle 110 \rangle$ stress may lead more rapidly to localization of the Cl_2^-, i.e., to smaller excursions away from the $\{110\}$ plane.

Finally, another observation which has not been dealt with so far is the apparent absence of any effect that $\langle 100 \rangle$ stress has on the lifting of the RIM tunneling motion.[3] An inspection of this with our model shows (i) that this can only be understood if there is indeed a large angle librational motion of the type we have been describing; and (ii) that the absence of a measurable quantitative effect is more or less accidental.

IV. SUMMARY AND CONCLUSIONS

We have shown that $\vec{\sigma} \| \langle 110 \rangle$ stress lifts the degeneracy of the three tunneling orientations involved in the RIM of the $H_A(Li^+)$ center, and two differential stress coupling coefficients $\beta_{[110]}$ and $\beta_{[1\bar{1}0]}$ were determined. Though these are insufficient to determine the orientation of the elastic dipole axes, an argument based on the expected size of the stress coupling coefficients for interstitial centers made it possible to conclude that one dipole axis, namely η, is close to a $\langle 111 \rangle$ direction. This axis is probably defined by the Li^+-interstitial Cl No. 1 direction (Fig. 8) which is expected to induce the major part of the elastic dipole and to determine its orientation.

The $\vec{\sigma} \| \langle 100 \rangle$ stress data and their temperature dependence[3] were interpreted (Sec. IV) in terms of a freely librating elastic dipole model. A quantitative description of the data is possible if it is assumed that, without stress, the Cl_2^- librates along an almost quadrant of a cone around $\langle 100 \rangle$ whose apex angle is $2 \times 28.2°$ (Fig. 1). This large-angle librational motion (LM) must have a libration frequency of at least 5×10^9 Hz in order to yield the observed motionally averaged, but still anisotropic, ESR spectra. A linear stress coupling coefficient $\beta^{LM}_{[001]}$ of expected size was obtained and this made possible a better fix of the principal axis and principal values of the elastic dipole tensor $\vec{\lambda}'$.

This large-angle LM of C_{1h} symmetry is a third distinct motion of the $H_A(Li^+)$ center which must be added to the already established[2] restricted interstitial motion (RIM) of C_{3v} symmetry around $\langle 111 \rangle$ and the pyramidal motion (PM), of C_{4v} symmetry around $\langle 100 \rangle$. The conclusions regarding the LM obtained in this paper replace the conclusions given in a recent note in which the existence of a small-angle librational motion was argued.[5]

The observation in the latter reference, namely a slight loss of resolution and broadening of the ESR lines at 4.2 K compared to 15 K, may be explained as an attempt towards localization of the Cl_2^- in the neighborhood of the (011) plane, possibly brought about by a temperature-induced curvature near (011) of the rather flat potential the Cl_2^- is moving in.

TABLE III. Raw ESR data of $H_A(Li^+)$ in KCl:Li^+ at 14 K. (a) Without second-order corrections; (b) with second-order correction.

Direction of magnetic field $\vec{H}$	g factors	Hyperfine splittings in gauss $(g_0/g)K_1$	$(g_0/g)K_2$
$\langle 100 \rangle + 26°$ in $\{110\}$	(a) 2.0031 (b) 2.0028	104.8	96.8
$\langle 100 \rangle$	(a) 2.0093 (b) 2.0089	91.2	91.2
$\langle 111 \rangle$	(a) 2.0088 (b) 2.0080	95.6	79.1
$\langle 110 \rangle$	(a) 2.0097 (b) 2.0084	89.1	82.3

TABLE IV. Illustration of the "static" fit to the $H_A(Li^+)$ ESR data using the extrapolated $A_\perp^2$ values (in units of G^2) as a criterion. (i) Requiring that $\Sigma = \theta^i_{\langle 100\rangle} + \theta^i_{\langle 111\rangle} = 54.74°$; (ii) not requiring that $\Sigma = 54.74°$. The fit is seen to be bad.

Direction of $\vec{H}$	$g_\perp$	$A^2_{\perp,1}$ (i)	$A^2_{\perp,1}$ (ii)	$A^2_{\perp,2}$ (i)	$A^2_{\perp,2}$ (ii)
⟨100⟩	2.0298 [a]	0 [b]	−1300 [c]	0 [d]	−13 000 [e]
⟨111⟩	2.0298 [a]	0 [b]	−1800 [c]	0 [d]	−1300 [e]
⟨110⟩	2.0234		−2300 [f]		−400 [f]

[a] $\theta''_g = 28.5° \pm 0.1°$. This value corresponds to g_x.
[b] For this $A_{\perp,1} = 0$ value, $\Sigma = 58.7°$ instead of 54.74°.
[c] For these unacceptable $A^2_{\perp,1}$ values, $\theta'_1 \equiv \theta^1_{\langle 100\rangle} = 30.4°$ and $\theta^1_{\langle 111\rangle} = 24.3°$ giving $\Sigma = 54.7°$.
[d] For this $A_{\perp,2} = 0$ value, $\Sigma = 59.7°$ instead of 54.74°.
[e] For these unacceptable $A^2_{\perp,2}$ values, $\theta'_2 \equiv \theta^2_{\langle 100\rangle} = 18.5°$ and $\theta^2_{\langle 111\rangle} = 36.2°$ giving $\Sigma = 54.7°$.
[f] These unacceptable $A^2_\perp$ values were calculated using $\theta^1_{\langle 100\rangle} = 30.4°$ and $\theta^2_{\langle 100\rangle} = 18.5°$.

Although the Cl_2^- moves in a flat potential while librating, it must encounter rather steep potential walls when it approaches the {100} planes. Indeed, it cannot cross a {100} plane at 4.2 K for if it did, the pyramidal motion would already exist at 4.2 K and this, together with the tunneling RIM, would make it impossible to produce an optical anisotropy at 4.2 K.[1,2] The steep potential walls are surmounted only at and above 23.5 K which is the disorientation temperature of the PM.[2]

The existence of a fast LM ($\gtrsim 5\times10^9$ Hz) offers a possibility of explaining the rather short spin-lattice relaxation time T_1 of the $H_A(Li^+)$ center. This T_1 was, very roughly, estimated to be 5×10^{-5} sec. An attempt to link this short T_1 to the RIM ran into an apparent quantitative difficulty[2]: almost every jump of the RIM should induce a spin flip, and this seems rather unlikely. However, the large-angle LM established in this paper has a libration frequency which is many orders of magnitude faster than the RIM frequency. Thus the fast LM could very well be at the basis of the short T_1.

Another observation which finds a natural explanation as a result of the large-angle LM is that the ESR line-broadening temperatures caused by the RIM are the same within experimental error, for both the stressed and the unstressed $H_A(Li^+)$ centers, namely[3] $T_{LB}(RIM) = 29$ K. The applied stress merely induces a change in the average Cl_2^- orientation along the librational path. Consequently, it does not prohibit the occurrence of the RIM, and it should not substantially affect the $T_{LB}(RIM)$.

Although the model of the freely librating elastic dipole is quite successful in describing the uniaxial stress data it is possible that more accurate measurements may emphasize the quantitative discrepancies; but it is also possible that such measurements agree better with each other and with the predicted behavior. If more accurate stress measurements along both ⟨100⟩ and ⟨110⟩ would confirm a quantitative discrepancy with the model, then the explanation must very likely be sought in the localization of the Cl_2^- axis brought about by stress-induced strain around the center which, because of the strong anisotropy of the compliance, depends on the stress orientation. Furthermore, a temperature dependence of the principal values of the elastic dipole tensor remains a distinct possibility.

ACKNOWLEDGMENTS

The authors want to thank P. H. Yuster, C. J. Delbecq, T. L. Gilbert, F. Lüty, G. D. Watkins, and A. M. Stoneham for fruitful discussions. A Nato research grant permitting additional experiments at ANL by both authors, and support from the Belgian science supporting agencies NFWO and IIKW are gratefully acknowledged.

APPENDIX: ANALYSIS OF ESR SPECTRUM OF FREELY LIBRATING ELASTIC DIPOLE

The evidence from the uniaxial stress data, especially the temperature dependence, that the Cl_2^- of the $H_A(Li^+)$ center is librating over a large angle is very compelling and constitutes a proof

TABLE V. Librational averages $\langle\cos^2\theta\rangle$, $\langle\sin\theta\cos\theta\cos\psi\rangle$, and $\langle\sin\theta\cos\theta\sin\psi\rangle$ for $\theta'' = 28.2°$ and a librational amplitude $\psi'_b - \psi''_a = 80°$. These values were used to obtain the $H_A(Li^+)$-center spin-Hamiltonian parameters of Table VII in which inequivalency of nuclei and bending of Cl_2^- bond was ignored. The θ_{eff} values were used for the calculation of the second-order hf shifts.

Direction of $\vec{H}$	$\langle\cos^2\theta\rangle$	$\langle\sin\theta\cos\theta\sin\psi\rangle$	$\langle\sin\theta\cos\theta\cos\psi\rangle$
⟨100⟩ + 26° in {110}	0.966 ($\theta_{eff} = 10.6°$)	0	0.026
⟨100⟩	0.777 ($\theta_{eff} = 28.2°$)	0	0.383
⟨111⟩	0.747 ($\theta_{eff} = 30.2°$)	0	0.402
⟨110⟩	0.715 ($\theta_{eff} = 32.3°$)	0.247	0.331

by itself. The ESR spectra, though still quite anisotropic, should reflect this large-angle LM. However, its presence is not obvious at a first glance and even an analysis based on the observed angular variation puts the Cl_2^- axis statically in a $\{110\}$ plane and making a 26° angle with $\langle 100\rangle$. We remarked already in Sec. III that, because the ESR spectra are well defined, the LM must be fast enough to give a motionally averaged but still anisotropic spectrum. The magnetic field interval over which the outer ESR lines are averaged is, on the average, of the order of 100–200 G. The librational frequency must therefore be of the order of, or larger than, 5×10^9 Hz.

The qualitative features of the ESR spectra do not yield the existence of a LM. Its presence can only be determined from a careful quantitative analysis based on accurate measurements.

Thus we will perform both a "static" analysis based on formulas (22) and (23), and a "librational" analysis based on formulas (19)–(21). Then we will compare them to see which one gives a better fit. A visually convincing procedure would be to calculate the angular variation for the two cases and compare them with the experimental angular variation. However, for nonspecial directions of $\vec{H}$, the spectra are oftentimes not sufficiently well resolved, and so the analysis will be based on the results of careful measurements along four particular directions: $\vec{H}\parallel\langle 110\rangle$, $\vec{H}\parallel\langle 100\rangle$, $\vec{H}\parallel\langle 111\rangle$ and $\vec{H}\parallel(\langle 100\rangle + 26°$ in $\{110\})$. The observed hf separation is maximum for the latter direction.

For each of these directions one wants the following parameters (in an axial approximation): the g factor, and the first-order hf separation K_i. We are assuming that the two Cl nuclei of the Cl_2^- are inequivalent and that their hf tensor symmetry axes do not coincide with each other (i.e., the molecular bond is bent) or with the g-tensor symmetry axis.

TABLE VI. Illustration of the "librational" fit to the $H_A(Li^+)$ ESR data, in which inequivalency of the nuclei and bending of the molecular bond is ignored. Using the extrapolated $A_\perp$ values (in gauss units) as a criterion, the fit is seen to be quite good. The value obtained for θ'' is 28.2°. This analysis gives the sign of $A_\perp$.

Direction of $\vec{H}$	$g_\perp$	$A_\perp$
$\langle 100\rangle$	2.033	+13.1
$\langle 111\rangle$	2.025	+13.1
$\langle 110\rangle$	2.023	+12.0

These parameters for the four orientations are summarized in Table III, and they were obtained as follows. From the difference between the uppermost and the lowest lines one obtains $(g_0/g)(K_1+K_2)$. From the average of the two differences (uppermost minus next-uppermost line) and (lowest minus next-lowest line) one obtains $(g_0/g)K_2$, and hence $(g_0/g)K_1$. By making these differences and averages, second order effects are eliminated. The mean position of the uppermost line and lowest line defines g, but uncorrected for important second-order shifts. Table III also gives the g's corrected for second-order shifts. Here a little explanation is necessary because, depending on the type of analysis one is performing, one needs "static" or "librational" second-order corrections. An investigation of this matter learns that both types of shifts are comparable to one another, except for the case $\vec{H}\parallel(\langle 100\rangle + 26°$ in $\{110\})$, where in the "static" case the correction is negligible while in the "librational" case it amounts to 0.0003. The corrected g values in Table III are based on "librational" second-order shifts because this type of analysis turns out to be the better one. These shifts were approximated employing the formulas used for "static" shifts and using an effective θ_{eff}

TABLE VII. Spin-Hamiltonian parameters of $H_A(Li^+)$ in KCl:Li^+ at 14 K obtained by a "librational" analysis. (i) Including bending of Cl_2^- molecular bond and inequivalency of nuclei; (ii) ignoring bending and inequivalency. The hyperfine values are given in gauss.

	$g_{z''}$	$g_{x''}$	$g_{y''}$	$A_{\parallel,1}$	$A_{\parallel,2}$	$A_{\perp,1}$	$A_{\perp,2}$	Bending angle $\theta_1'' - \theta_2''$
(i)	2.0018[a] ±0.0002	2.031[b] ±0.001	2.025 ±0.001	+108.9[c] ±0.1	+99.1[d] ±0.1	+14.5 ±3.5	+9.2 ±1.7	10.8° ±0.4°
(ii)	2.0019[e] ±0.0002	2.029 ±0.001		+103.6[e] ±0.1		+12.5 ±2		0°

[a] $\theta_g'' = 29.2° \pm 0.2°$ in the Cl_2^--Li^+ plane.
[b] x'' axis is perpendicular to the internuclear Cl_2^- axis z'' and lies in Cl_2^--Li^+ plane.
[c] $\theta_1'' = 32.1° \pm 0.1°$ in the Cl_2^--Li^+ plane.
[d] $\theta_2'' = 21.3° \pm 0.3°$ in the Cl_2^--Li^+ plane.
[e] $\theta'' = 28.2° \pm 0.1°$ in the Cl_2^--Li^+ plane.

TABLE VIII. Librational averages for $\langle\cos^2\theta\rangle$, $\langle\sin\theta\cos\theta\cos\psi\rangle$, and $\langle\sin\theta\cos\theta\sin\psi\rangle$ for the two hyperfine tensors ($\theta_1'' = 32.1°$ and $\theta_2'' = 21.3°$) and the g tensor ($\theta_g'' = 29.2°$). The librational amplitude corresponds to $\psi_b'' - \psi_a'' = 80°$. The averages were used to obtain the spin-Hamiltonian parameters in Table VII. $i = 1, 2, g$, going down in that order.

Direction of $\vec{H}$	$\langle\cos^2\theta_i\rangle$	$\langle\sin\theta_i\cos\theta_i\sin\psi_i\rangle$	$\langle\sin\theta_i\cos\theta_i\cos\psi_i\rangle$
$\langle 100\rangle + 26°$ in $\{110\}$	0.952	0	0.069
	0.970	0	0.089
	0.964	0	0.032
$\langle 100\rangle$	0.718	0	0.411
	0.868	0	0.309
	0.762	0	0.389
$\langle 111\rangle$	0.790	0	0.360
	0.652	0	0.455
	0.759	0	0.391
$\langle 110\rangle$	0.723	0.277	0.286
	0.688	0.188	0.398
	0.718	0.255	0.318

derived from the $\langle\cos^2\theta\rangle$ values (see Table V).

In order to decide which of the two analyses gives the best fit the following procedure will be applied. First, from the $\vec{H} \parallel (\langle 100\rangle + 26°$ in $\{110\})$ spectrum, values for $g_\parallel$, $A_{\parallel,1}$, and $A_{\parallel,2}$ are determined. Using these, the values for $g_\perp$, but especially $A_{\perp,1}$ and $A_{\perp,2}$ will be calculated from the data of each of the other three special $\vec{H}$ directions. If the fit is good, this procedure will yield good $A_\perp$ values. The hyperfine components of the Cl_2^- V_K and H centers are very well known[15,18]: the $A_\perp$ values vary between + 5 to + 16 G. So values in this range will be considered as good.

"Static" analysis. The $\vec{H} \parallel (\langle 100\rangle + 26°$ in $\{110\})$ data of Table III yield immediately $g_\parallel = 2.0031$ in this case, because second-order corrections are negligible for $\theta = 0°$. In case of no bending of the molecular bond, the two K values would give immediately $A_{\parallel,1}$ and $A_{\parallel,2}$. However, we shall see that the total bending is about 12°. Consequently, $A_{\parallel,1} \cong K_1/\cos 6° = 105.3$ G and $A_{\parallel,2} \cong K_2/\cos 6° = 97.2$ G.

We can now treat the $\vec{H} \parallel \langle 100\rangle$ and $\vec{H} \parallel \langle 111\rangle$ data together. Using formula (22) we can solve for $A_{\perp,i}$, $\theta^i_{\langle 100\rangle}$, and $\theta^i_{\langle 111\rangle}$ in which $\theta^i_{\langle 100\rangle}$ is the angle that $\vec{H} \parallel \langle 100\rangle$ makes with the hf tensor axis i, and similarly $\theta^i_{\langle 111\rangle}$ for $\vec{H} \parallel \langle 111\rangle$. We note that $\theta^i_{\langle 100\rangle} + \theta^i_{\langle 111\rangle} = 54.74°$ is a necessary condition. Solutions are found for $\theta^1_{\langle 100\rangle}$ and $\theta^2_{\langle 100\rangle}$ (see Table IV) but in both cases one finds strongly negative values for $A^2_{\perp,1}$ and $A^2_{\perp,2}$. This is impossible and indicates a bad fit. Using these θ^1 and θ^2 values one can analyze the $\vec{H} \parallel \langle 110\rangle$ data. Again strongly negative $A^2_\perp$ values are found.

This "static" analysis gives a bad fit for the ESR spectra. The best one could say in this analysis is that $A_{\perp,1} \approx A_{\perp,2} = 0$ G. Conversely, if one accepts the latter values, the condition $\theta^i_{\langle 100\rangle} + \theta^i_{\langle 111\rangle} = 54.74°$ cannot be fulfilled as is made clear in Table IV.

As far as the g factors are concerned, we note that $g_{\langle 100\rangle}$ and $g_{\langle 111\rangle}$ should extrapolate to the same g_x value. We find $g_x = 2.0298$ with $\theta_g'' \equiv \theta^g_{\langle 100\rangle} = 28.5° \pm 0.1°$. From the $\langle 110\rangle$ data one finds $g_y = 2.023$. The total bending is $\theta_1'' - \theta_2'' = 30.4° - 18.5° \cong 12°$. The results of the "static" analysis as given in this section replace the values obtained earlier.[1,2]

"Librational" analysis. We will present two analyses in which the LM is taken into account. In the first one, we will ignore inequivalency of the nuclei and bending of the molecular bond; in the second one, these will be taken into account. The reason for presenting the first one at all is

TABLE IX. Illustration of the "librational" fit to the $H_A(Li^+)$ ESR data in which the inequivalency of the nuclei and bending of the Cl_2^- bond is taken into account. Using the extrapolated $A_{\perp,i}$ values (in gauss units) as a criterion, the fit is seen to be good. Note that this analysis gives the signs of $A_{\perp,1}$ and $A_{\perp,2}$.

Direction of $\vec{H}$	$g_\perp$	$A_{\perp,1}$	$A_{\perp,2}$
$\langle 100\rangle$	2.0315 [a]	+17.1 [b]	+7.9 [c]
$\langle 111\rangle$	2.0274 [a]	+17.1 [b]	+7.9 [c]
$\langle 110\rangle$	2.0251	+9.2	+11.9

[a] Corresponds to $\theta_g'' = 29.2°$. In the "librational" analysis these values need not be equal. The 2.0315 value corresponds to g_x.

[b] Corresponds to $\theta_1'' = 32.1° \pm 0.1°$.

[c] Corresponds to $\theta_2'' = 21.3° \pm 0.3°$.

that similar motions may exist in other Cl_2^--type centers for which it is often impossible or difficult to obtain accurate K_1 and K_2 values, but only $\frac{1}{2}(K_1+K_2)$. If the first type of analysis would give reasonable results one would feel confident in analyzing other centers in this approximation. For the "librational" analyses formulas (19)–(21) are used, the latter with $\sigma=0$. The uniaxial stress data have suggested (Sec. III) that the librational amplitude is $\psi_b''-\psi_a''=70°$–$80°$, in other words, the Cl_2^- approaches the {100} planes not closer than 5° or 10°. The integrals for $\langle\cos^2\theta_i\rangle$ and $\langle\sin\theta_i\cos\theta_i\sin\psi_i\rangle$ can be carried out analytically and one finds

$$\langle\cos^2\theta_i\rangle = a_i^2+\tfrac{1}{2}b_i^2+[b_i/(\psi_b''-\psi_a'')][a_i(\sin\psi_b''-\sin\psi_a'')+\tfrac{1}{4}b_i(\sin2\psi_b''-\sin2\psi_a'')]\,, \tag{A1}$$

$$\langle\sin\theta_i\cos\theta_i\sin\psi_i\rangle = [\sin\theta_i''/(\psi_b''-\psi_a'')][a_i(\cos\psi_a''-\cos\psi_b'')+\tfrac{1}{4}b_i(\cos2\psi_b''-\cos2\psi_a'')]\,, \tag{A2}$$

with $(i=1,2,g)$

$$a_i=\cos\theta_i''\cos\theta'\,,\quad b_i=\sin\theta_i''\sin\theta'\,, \tag{A3}$$

in which θ_i'' is the constant angle that the $\vec{K}_i$- or $\vec{g}$-tensor axis make with [001] and θ' is the angle that $\vec{H}$ makes with [001]. The angle θ_i is between $\vec{H}$ and the tensor axis.

The values of $\langle\sin\theta_i\cos\theta_i\cos\psi_i\rangle$ were calculated numerically on an HP-25 programmable pocket calculator.

For the analysis in which the equivalency of the nuclei and the bending of the Cl_2^- bond is ignored, the foregoing formulas were used with $\theta\equiv\theta_1\equiv\theta_2\equiv\theta_g$. After a lengthy analysis it was found that a good fit was obtained with $\theta''=28.2°\pm0.1°$. Table V gives the librational averages $\langle\cos^2\theta\rangle$, etc., ..., for this θ'' angle. Table VI illustrates the fit (it is quite good), and Table VII gives the spin-Hamiltonian parameters in this approximation.

In the analysis in which inequivalency of the nuclei and bending of the Cl_2^- bond is taken into account, θ_1'', θ_2'', θ_g'' are permitted to have different values. A lengthy analysis finally yielded the following values: $\theta_1''=32.1°$, $\theta_2''=21.3°$, and $\theta_g''=29.2°$. The resulting librational averages $\langle\cos^2\theta_i\rangle$ etc., ..., are summarized in Table VIII. Table IX illustrates the fit to the ESR data using the sign and values of $A_{\perp,i}$ as a criterion; the fit is seen to be quite good. It should be stressed that the "librational" analysis gives the sign of $A_{\perp,i}$ (the sign of $A_{\parallel,i}$ is known[18]) something the "static" analysis cannot.

The spin-Hamiltonian parameters obtained from this "librational" fit are also given in Table VII. They are distinctly different from, and superior to, the spin-Hamiltonian parameters obtained from the "static" analysis. It should also be remarked that the two "librational" analyses are quite consistent with one another.

*Based on work performed under the auspices of the U. S. Energy Research and Development Administration.

†Permanent address.

[1]D. Schoemaker and J. L. Kolopus, Phys. Rev. B 2, 1148 (1970).

[2]D. Schoemaker and E. L. Yasaitis, Phys. Rev. B 5, 4970 (1972).

[3]D. Schoemaker, Phys. Rev. B 9, 1804 (1974).

[4]D. Schoemaker, Bull. Am. Phys. Soc. 10, 305 (1973).

[5]D. Schoemaker, Phys. Rev. B 12, 715 (1975).

[6]L. Brillouin, *Tensors in Mechanics and Elasticity* (Academic, New York, 1964).

[7]A useful review of the theory of elastic solids in the presence of defects is A. S. Nowick and W. R. Heller [Adv. Phys. 12, 251 (1963)].

[8]K. Bachmann and W. Känzig, Phys. Kondens. Mater. 7, 204 (1968).

[9]L. Landau and E. Lifchitz, *Théorie de l'Elasticité* (MIR, Moscow, 1967).

[10]W. Plant and R. L. Mieher, Phys. Rev. B 7, 4793 (1973).

[11]A. Lagendijk and D. Schoemaker (unpublished results); D. Schoemaker, in Proceedings of the International Conference on Color Centers in Ionic Crystals, Sendai, Japan, 1974 (unpublished).

[12]R. Balzer, H. Peters, W. Waidelich, and H. Peisl, Phys. Rev. B 9, 2746 (1974).

[13]The librational angle γ can be fixed by making a very-large-temperature and a very-small-temperature asymptotic expansion of Eq. (15).

[14]*Handbook of Mathematical Functions*, edited by M. Abramowitz and I. A. Stegun (Dover, New York, 1968).

[15]D. Schoemaker, Phys. Rev. B 3, 3516 (1971).

[16]The expression "change in geometry" is in the spirit of Ref. 3. In the spirit of the present paper it means a change in average orientation along the libration path.

[17]The KCl compliance coefficients can be calculated from the stiffness constants given by C. Kittel [*Introduction to Solid State Physics*, 4th ed. (Wiley, New York, 1971), p. 149].

[18]D. Schoemaker, Phys. Rev. B 7, 786 (1973).